Imidazole for Pyridine Substitution Leads to Enhanced Activity Under Milder Conditions in Cobalt Water Oxidation Electrocatalysis

Noah D. McMillion,[a‡] Amanda W. Wilson,[a‡] McKenna K. Goetz,[a] Mu-Chieh Chang,[a†] Chia-Cheng Lin,[b] Wei-Jie Feng,[b] Charles C. L. McCrory,[b] and John S. Anderson[a*]

[a]Department of Chemistry, University of Chicago, 929 E. 57th St, Chicago, IL 60637

[b]Department of Chemistry, University of Michigan, 930 N. Michigan Ave., Ann Arbor, MI 48109

Supporting Information Placeholder

ABSTRACT: A previously reported cobalt complex featuring a tetraimidazolyl-substituted pyridine chelate is an active water oxidation electrocatalyst with moderate overpotential at pH 7. While this complex decomposes rapidly to a less-active species under electrocatalytic conditions, detailed electrochemical studies support the agency of an initial molecular catalyst. Cyclic voltammetry measurements confirm that the imidazolyl donors result in a more electron-rich Co center when compared with previous pyridine-based systems. The primary changes in electrocatalytic behavior of the present case are enhanced activity at lower pH and a marked dependence of catalytic activity on pH.

Introduction

Water oxidation converts water to oxygen, making it attractive in the development of systems that store energy from renewable sources.[1-3] There are two primary challenges associated with efficient water oxidation: the high oxidation potential required to drive this reaction (1.23 V vs. NHE at standard conditions), and the coordinated movement of two molecules of water, four electrons, and four protons.[4-6] Currently, some of the most effective catalysts for this process are heterogeneous precious metal oxides that operate under basic conditions.[7-9] To avoid the use of expensive catalysts under harsh conditions, significant effort has been directed at the utilization of inexpensive metal catalysts, preferably those which operate at a mild pH.[7-14] The heterogeneous nature of many catalyst materials, however, often complicates their mechanistic study.[15-21] The above challenges motivate the design of molecular water oxidation catalysts using abundant first row transition metals such as Cu, Co, Fe, or Mn. While molecular systems featuring precious metals have been studied in detail,[22-28] there have been comparatively fewer studies on first row transition metal catalysts.[23-25, 29-34] The study of these types of molecular catalysts is therefore important as it allows for systematic alteration in order to test the impact of various design principles.

There are some limited examples in the current literature of molecular Co systems capable of carrying out water oxidation.[35-41] Some early reports of Co-based molecular systems for water oxidation utilized the well-known penta-pyridyl Py5 donor scaffold, a ligand which can also be used in systems carrying out proton reduction (complex **1**, Figure 1).[42-47] Modification of the arms in this pentadentate scaffold should allow for rational tuning of catalytic properties. Indeed, stronger

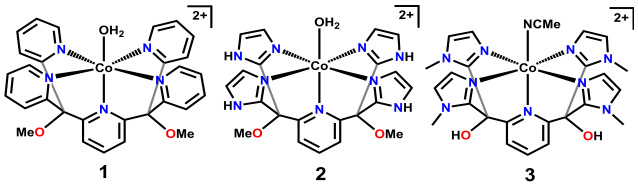

Figure 1. N5 tetrapodal Co systems giving rise to water oxidation catalysis.

imidazole donors have already been pursued as represented by complex **2** (Figure 1).[48,49] Unfortunately, this specific complex suffers from aqueous insolubility from pH 7 to pH 11 due to charge neutralization by deprotonation of the cationic complex, complicating comparisons of its catalytic activity with the Py5-based system. A closely related ligand scaffold is the methylated analogue tip(Me) (tip(Me) = 2,6-(bis(bis-2-*N*-methylimidazolyl)-hydroxymethyl)pyridine), which was reported nearly 40 years ago, but has not been examined for water oxidation catalysis (complex **3**, Figure 1).[50,51]

In this work, we show that metalation of tip(Me) with Co^{II} yields a complex that is an active electrocatalyst for water oxidation from pH 7-9. While this catalyst decomposes rapidly under electrolysis, a suite of detailed studies supports the agency of an initial molecular species. Several differences are apparent between the electrocatalytic activity of **1** and **3**. Complex **3** displays enhanced catalytic activity at milder pH values than **1**. Furthermore, the peak current and potential of **3** are pH dependent unlike **1**. The pH dependence of these features suggests a rate-determining PCET step for catalysis. This observation is inconsistent with the experimentally proposed mechanism for **1** but may support a pathway involving formation of a formal Co(IV)-oxo intermediate previously suggested by computational studies.[47] These observations underscore that even minor perturbations of the catalyst structure of N5 ligated Co complexes may change the electrocatalytic mechanism.

Results and Discussion

Synthesis of the tip(Me) ligand (Scheme 1) was modified from previously reported procedures.[50,51] Metalation was carried out by adding an acetonitrile suspension of the ligand dropwise to $[Co^{II}(MeCN)_6][OTf]_2$, yielding an orange solution of $[Co^{II}(tip(Me))(MeCN)][OTf]_2$, complex **3**. Crystallization of the complex by vapor diffusion of diethyl ether into acetonitrile yielded orange-colored single crystals suitable for X-ray diffraction studies.

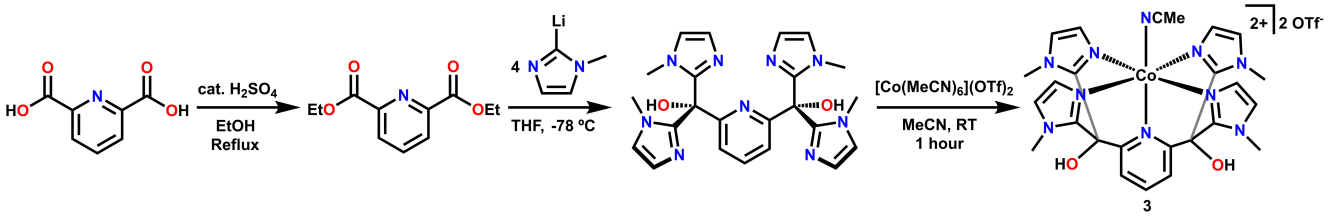

Scheme 1. Synthesis of $[Co^{II}(tip(Me))(MeCN)][OTf]_2$, **3**.[50,51]

The crystal structure of complex **3** (Figure 2) confirms the assignment of the complex as a mononuclear acetonitrile adduct with outer sphere triflate counter-anions. Bond distances between Co and the imidazolyl/pyridyl donors for complex **3** average 2.09 Å, which is similar to those of the previously-reported tetraimidazolyl pyridine system (2.10 Å, complex **2**) but somewhat shorter than the analogous pentapyridine Co complex (2.16 Å, complex **1**), as might be expected due to differences in the donating abilities of the pyridyl and imidazolyl ligands.[44,49] Complex **3** shows characteristically shifted paramagnetic peaks in its ^{1}H NMR spectrum, consistent with a C_{2v}-symmetric complex in solution (See SI). Furthermore, EPR spectroscopy indicates that the Co^{II} center is high spin with a highly-rhombic $S = 3/2$ signal (See SI).

We briefly investigated the ability of complex **3** to bind O_2 due to previous reports of O_2 binding affinity in this system. When O_2 is bubbled through a pale orange solution of complex **3** the color of the solution rapidly changes to deep red.[50,51] The generated species is assigned as a mononuclear Co^{III}-superoxo complex ($[Co^{III}(tip(Me))(O_2^{-})][OTf]_2$, complex **4**), based on previous reports and spectroscopic data.[50,51] Monitoring this reaction by ^{1}H NMR spectroscopy shows the disappearance of the paramagnetic features attributed to complex **3** with no apparent growth of new features (See SI). This observation is consistent with the formation of an NMR-silent radical and supports the assignment of complex **4** as a Co^{III}-superoxo complex. UV-vis spectra recorded with subsequent additions of approximately two equivalents of O_2 also supports formation of a new species with a strong absorbance feature at 500 nm and a lower-intensity feature at approximately 300 nm, again consistent with previous reports (See SI).[50,51] Purging with N_2 results in the disappearance of these absorbance features as the sample reverts to **3**, highlighting the reversibility of O_2 binding (See SI). Characterization of complex **4** by EPR spectroscopy shows a small feature at low field attributed to residual complex **3** and an intense $S = 1/2$ feature near $g = 2$ that is consistent with the proposed complex containing a low-spin Co^{III} center and a superoxo-based radical (See SI).[50,51] Taken together these data support the formation of a superoxo complex upon addition of O_2 or air to solutions of complex **3**. The ability of **3** to bind O_2 highlights the effect of the donating imidazolyl arms in the tip(Me) system. All subsequent electrochemical analyses with complex **3** were conducted under anaerobic conditions to avoid convolutions from mixtures of **3** and **4** in solution.

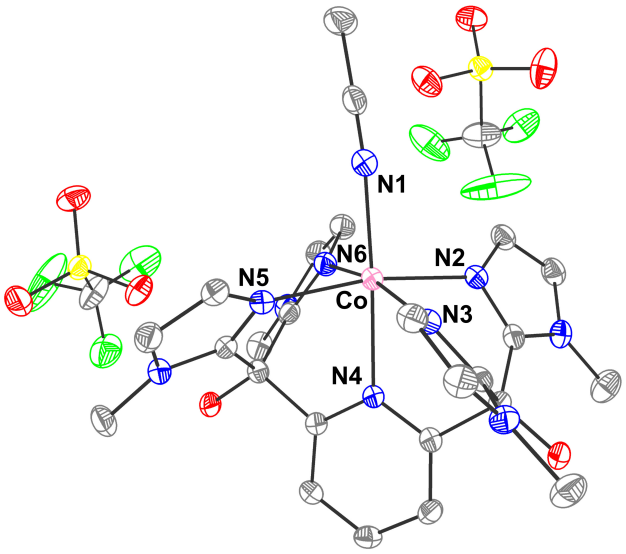

Figure 2. Solid-state structure of complex **3**. Selected bond lengths: Co-N1 2.116(2) Å, Co-N2 2.076(2) Å, Co-N3 2.097(2) Å, Co-N4 2.287(2) Å, Co-N5 2.094(2) Å, Co-N6 2.101(2) Å. H-atoms and exogenous solvent molecules omitted for clarity. Co shown in pink, S in yellow, F in green, O in red, N in blue, and C in gray.

The more electron-rich nature of complex **3** was also verified via electrochemical analysis. In aqueous pH 7 solution under a N_2 atmosphere, complex **3** shows a reversible couple at 0.202 V vs. NHE (See SI). This feature is assigned as a Co^{II}-OH_2 to Co^{III}-OH proton-coupled electron transfer (PCET) oxidation event as compared with an analogous couple at ~0.5 V vs. NHE in the well-characterized Py5 system.[44-47] This Co^{II}/Co^{III} couple in complex **3** shifts by 0.053 V/pH unit, which also suggests the presence of a PCET process (See SI). Scanning to more positive potentials shows a large increase in current, consistent with electrocatalytic water oxidation. This electrocatalytic wave shows a marked dependence on pH, with dramatic changes in current and peak potential upon moving from pH 6 to pH 9 (Figure 3).

The previously reported Py5 based catalyst **1** operates with an overpotential of ~0.5 V at pH = 9.2 defined from catalytic onset. An increase in peak current was observed upon increasing pH, but the electrocatalytic peak potential was largely invariant of pH. In the present system a similar overpotential of ~0.5 V is observed. Unlike complex **1**, however, the peak current of **3** increases with increasing pH, but drops sharply above

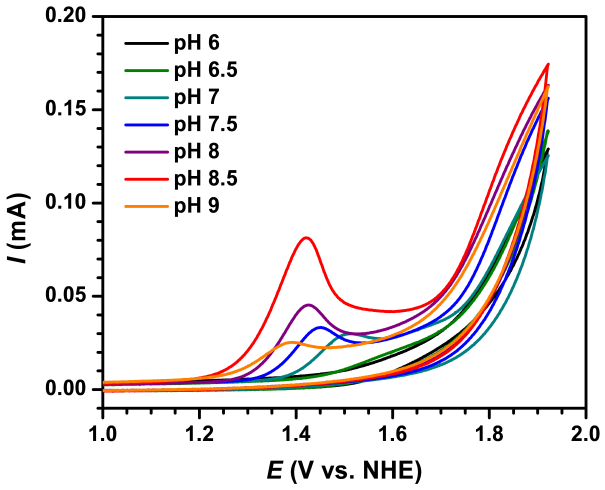

Figure 3. Variable-pH CV studies of complex **3** showing the catalytic current in 0.1 M sodium phosphate buffer, 0.5 mM complex **3**. Scan rate: 0.05 V/s.

pH 8.5. At comparable pH values of 8-8.5, complex **3** shows enhanced electrocatalytic activity when compared with **1** as evidenced by roughly 2x higher peak currents. The maximum peak current of **3** at pH = 8.5, however, is very similar to that observed for **1** (at pH = 9.8). What these data suggest is that catalyst **3** is more active than **1** at milder pH, but may be destabilized or inhibited by more basic conditions.

The production of O_2 and the Faradaic efficiency of this process were verified with *in situ* measurements using a Clark-type submersion O_2 probe.[8] These experiments show 84 ± 11% Faradaic efficiency for O_2 evolution and a decay in O_2 evolution activity over roughly 10 minutes (See SI). This decay suggests some degree of catalyst degradation. The apparent instability of complex **3** under catalytic conditions in this experiment, as well as the noted instability of related systems,[23,52-56] prompted us to more carefully evaluate whether the activity of complex **3** was simply due to decomposition or a bona-fide molecular species.

The possible involvement of heterogeneous species in homogeneous water oxidation has been well-documented.[23, 52-56] Cobalt-based systems are particularly susceptible to this, as Co^{II} ions are intermediates in the formation of heterogeneous CoO_x films or nanoparticles that exhibit water oxidation activity. To compare the electrochemical behavior of aqueous Co^{II} ions and complex **3**, cyclic voltammetry was also carried out in aqueous solutions of Co^{II} ions from pH 6 to pH 9 (See SI). While electrocatalytic waves are observed in the same region as those observed in complex **3**, the peak potentials of these waves are distinct and the absolute current values are quite different (~0.5 A for Co^{II} ions vs. ~0.08 A for **3** at pH 8.5). These observations support the molecular nature of **3**. The electrochemical activity of complex **3** was also compared to aqueous Co^{II} ions in the presence of a catalyst poison, 2,2'-bipyridine (bipy, See SI). The activity of complex **3** is completely shut down with just one equivalent of bipy, while the activity of aqueous Co^{II} ions was shut down only after the addition of three equivalents. These poisoning experiments also support the agency of a homogeneous species other than free Co^{II} ions.

To reconcile the homogeneity of this system with the proposed degradation, further control experiments were performed. Controlled potential electrolysis experiments were carried out on a solution of **3**, a solution containing $CoCl_2$, and a blank electrolyte solution with an electrode with CoPi deposited on its surface. The electrolysis of **3** resulted in the deposition of a film on the electrode. The electrocatalytic activity of this film was also analyzed. While aqueous $CoCl_2$ and complex **3** display similar bulk activity, the film resulting from decomposition of **3** and the CoPi film both show differing activity, suggesting that decomposition is not responsible for the catalysis observed for solutions of **3** (See SI).[10,15] To further corroborate this conclusion, a ten-minute bulk electrolysis at 1.45 V vs. NHE of a solution of complex **3** was performed at pH 7, followed by the removal of the solution from the cell and insertion of fresh electrolyte solution into the cell before collecting another CV scan (See SI). The data show that the features associated with electrochemical activity of complex **3** were not observed. However, an earlier electrocatalytic onset potential than a freshly-cleaned electrode was observed. Taken together, these data support the hypothesis that complex **3** operates as a molecular water oxidation catalyst but decomposes under the applied conditions to generate heterogeneous CoO_x species that are less active for water oxidation.

We have also carried out further studies on the film resulting from the decomposition of complex **3**. Characterization of this deposit, prior to rinsing, was carried out via X-ray photoelectron spectroscopy (XPS) and several control experiments. The specifics of the measurements and findings are discussed in detail in the SI, but in short, two main findings suggest that the cobalt deposit is likely a cobalt oxide and not intact complex **3**: 1) the peak positions of the Co $2p_{3/2}$ and Co $2p_{1/2}$ and their associated satellite peaks are similar to those expected for Co^{2+}/Co^{3+} oxidation states observed in cobalt oxide materials, and 2) the XPS measurements show a low N:Co ratio suggesting that the majority of the deposited Co is not part of intact complex **3** (See SI). Controlled potential electrolysis of the film immediately after XPS analysis shows that the film is active for water oxidation, though significantly less active than complex **3** consistent with previous observations. Furthermore, the electrolysis of intentionally-deposited CoPi shows more activity than the decomposition product of complex **3**, suggesting that the decomposition film is not composed of CoPi. All the control experiments performed here support that **3** operates as a distinct homogeneous water oxidation catalyst that is unstable under electrolysis conditions resulting in the deposition of a heterogeneous species, likely CoO_x. As previously noted,[52-56] it is still difficult to exclude completely the agency of some heterogeneous species.

The activity of complex **3** and its comparison to the activity of the previously-reported Py5 Co system **1** merits some discussion. The mechanism of catalysis for $[(Py5)Co^{II}(H_2O)]^{2+}$ is proposed to involve an initial PCET to form $[(Py5)Co^{III}(OH)]^{2+}$, which occurs at ~0.5 V vs. NHE near pH 7. Subsequent catalytic onset in this Py5 system occurs ~1 V more positive and is independent of pH. The initially proposed mechanism based on experimental evidence invoked a rate-determining oxidation to form $[(Py5)Co^{IV}(OH)]^{3+}$, which then rapidly reacts to generate O_2 and regenerate $[(Py5)Co^{II}(H_2O)]^{2+}$.[44,46] Alternative computational studies proposed a more nuanced mechanism that involves the generation of $[(Py5)Co(O)]^{2+}$ as the active intermediate for O-O bond formation.[47] A key prediction from these computational studies is that the formation of the $[(Py5)Co(O)]^{2+}$ unit should occur via a pH dependent PCET step. It is worthwhile to reiterate that this predicted pH dependent catalytic wave was not experimentally observed.

We anticipated that a more-donating ligand scaffold would move a pH-independent catalytic onset to milder, i.e. less positive, potentials. This tip(Me) system has been shown to be more-donating than the previous Py5-based catalysts, as evidenced by the observed shifts in the Co^{II}/Co^{III} redox potential and increased O_2-binding affinity. However, the onset of catalysis occurs in the present imidazolyl-substituted system at ~1.4 V vs. NHE, which is comparable to the catalytic onset observed in the Py5 system. A detailed comparison of the activities of catalysts **1** and **3** is difficult as we do not have a clear mechanistic picture for either of these systems. Nonetheless, we are able to note two important distinctions. First, under identical solution and electrode conditions, the tetraimidazolyl system is more active, with currents twice those observed in the Py5 system between pH 8 and 8.5. Second, in the present system the electrocatalytic activity shows a marked dependence on pH. Indeed, plotting the catalytic peak potential vs. pH shows a reasonable linear fit with a slope of 0.055 V/pH unit (See SI). This value is close to that expected for a 1 e^-/1 H^+ PCET step.

To further probe the importance of proton transfer we performed deuterium labeling studies. A significant decrease in the catalytic peak current intensity is observed in D_2O compared to H_2O, providing a KIE value of ~6 (See SI). This observation supports that proton transfer is involved in the turnover

limiting step. Finally, we also wanted to investigate the potential involvement of phosphate in turnover as has been invoked in atom-proton transfer (APT) type mechanisms.[57] We varied the concentration of phosphate under constant ionic strength and observed an inhibitory effect (See SI). This argues against an APT type mechanism, and may be consistent with competitive phosphate binding.

These differences between the catalytic activity of **1** and **3**, in particular the dependence of the peak potential of the catalytic wave on pH, suggests that there is a fundamental mechanistic difference between the imidazolyl-substituted catalyst and the previously studied pyridyl version. Indeed, it is reasonable that slight perturbations in ligand design and operating conditions may favor one of multiple competing mechanistic pathways. It is difficult to concretely interpret mechanistic differences between these systems. We can speculate, however, on an explanation for the different pH dependence observed for **1** and **3**. In the case of **1** the weak pyridine donor set may make oxidation the turnover limiting step at all measured pH values. Alternatively, the more donating imidazolyl scaffold in **3** makes oxidation more facile and deprotonation more difficult. Faster oxidation and slower deprotonation manifests in what may be a turnover limiting PCET step in the catalysis instead of just an oxidation. This would be consistent with the above-mentioned theoretical proposals that invoke a PCET step to form a formally Co(IV)-oxo intermediate which is then active for oxygen evolution.[47]

Conclusion

To summarize, we report a new cobalt-based water oxidation catalyst capable of operating at neutral pH. Through a series of control experiments, catalysis was shown to be consistent with an initial molecular species. Oxygen evolution measurements verify the generation of O_2 and suggest that complex **3** operates with a high Faradaic efficiency. This catalytic activity was enhanced when compared with the closely related Py5-based system. Furthermore, a marked dependence of the electrocatalytic peak current on pH is observed. An alternative pathway for catalysis between **1** and **3** is likely, underscoring how even slight structural changes may lead to different catalytic mechanisms.

Experimental Details

Materials & Instrumentation

Manipulations of complex **3** were carried out under a dry N_2 atmosphere using an mBraun Unilab Pro glove box. Laboratory-grade deionized water was used. Acetonitrile was dried on a solvent purification system from Pure Process Technologies before storing over 4 Å molecular sieves under N_2. Tetrahydrofuran (THF) was stirred over NaK alloy and passed through a column of activated alumina before storing over 4 Å sieves under N_2. Synthesis of tip(Me) was carried out using a procedure modified from Tagaki, et. al. (see below).[51] Unless otherwise noted, reagents were obtained from commercial suppliers and used without further purification.

^{1}H NMR measurements were collected at room temperature on a Bruker DRX 400 MHz spectrometer. X-band EPR spectra were recorded on an Elexsys E500 Spectrometer with an Oxford ESR 900 X-band cryostat and a Bruker Cold-Edge Stinger. UV-Vis spectra were collected on a Thermo Scientific Evolution 300 UV-Vis spectrometer. X-ray photoelectron spectroscopy (XPS) measurements were conducted using a Kratos Ultra XPS instrument with a monochromatic Al X-ray source operating at 8 mA and 14 kV. All XPS data was analyzed using CasaXPS version 2.3.17 (Casa Software, Ltd.). Cyclic Voltammograms (CVs) were collected using a BAS Epsilon potentiostat and analyzed using BAS Epsilon software version 1.40.67NT. CV traces were analyzed in Origin (OriginLab, Northampton, MA) and smoothed as appropriate using the 5 points adjacent averaging function. Controlled-potential electrolyses were conducted using a Bio-Logic SP200 potentiostat, and data were recorded using the Bio-Logic EC-Lab V10.44 software package.

Synthesis of 2,6-bis(bis(2-imidazolyl)-methanol)pyridine (tip(Me)). 1-methylimidazole (3.3 g, 40 mmol) was dissolved in 250 mL THF under an inert atmosphere and cooled to –78 °C. A solution of n-butyllithium (2.5 M in hexanes, 16 mL, 40 mmol) was added and the mixture stirred for 45 minutes. Diethyl 2,6-pyridinedicarboxylate (2.23 g, 10 mmol), prepared according to literature procedures,[58] was added as a solution in THF and the reaction mixture was stirred overnight. The reaction mixture was pumped down to an off-white solid and dissolved in MeOH. NH_4NO_3 (3.20 g, 40 mmol) was dissolved in a minimal amount of de-ionized H_2O and added to the solution. MeOH was removed *in vacuo,* and the resulting solution was extracted with DCM and the organic layer dried using $MgSO_4$. The solvent was removed, and the ligand was recrystallized twice by layering $CHCl_3$ and hexanes. Pure off-white solid was obtained after washing with hot toluene (2.013 g, 4.38 mmol, 43.6%). The properties of tip(Me) are identical to those previously reported.[52] ^{1}H NMR (400 MHz; $CDCl_3$ δ): 7.87 (1H, t, py-4H), 7.63 (2H, d , py-3,5H), 6.90 (4H, d, im-4H), 6.81 (4H, d, im-5H), 6.12 (2H, s, OH), 3.16 (12H, s, CH_3).

Synthesis of $[Co^{II}(tip(Me))(MeCN)](OTf)_2$ (3). A slurry of tip(Me) (0.100 g, 0.218 mmol) in 5 mL of acetonitrile was slowly added to a 5 mL acetonitrile solution of $[Co^{II}(MeCN)_6](OTf)_2$ (0.132 g, 0.219 mmol). $[Co^{II}(MeCN)_6](OTf)_2$ was prepared following a literature procedure.[59] The resulting solution was stirred at room temperature for one hour and then purified by layering Et_2O on top of a concentrated solution of complex **3** in acetonitrile. An analytically-pure crystalline light orange solid was obtained after 12 hours (0.165 g, 0.192 mmol, 88%). ^{1}H NMR (400 MHz; CD_3CN δ): 73.16 (4H, s), 42.31 (4H, s), 28.60 (2H, s, py-3,5H), 26.83 (12H, s, CH_3), –13.04 (1H, s, py-4H). ESI-MS *m/z* 259.2 $[Co^{II}(tip(Me))]^{2+}$. Elemental analysis: expected for $CoC_{27}H_{28}N_{10}O_8F_6S_2$: % C: 37.81; N, 16.34; H, 3.30. Found: % C, 37.46; N, 16.16; H, 3.33.

$[Co^{III}(tip(Me))(O_2^-)](OTf)_2$ (4): Complex **4** was not isolated, but was instead generated *in situ* for each experiment. The generation of complex **4** can be easily identified by the color of the solution: complex **3** is colorless in an air-free solution, while complex **4** is a deep red. For spectroscopic measurements, oxygen was bubbled through a solution of complex **3**. The properties of complex **4** are analogous to those previously reported for the corresponding NO_3^- salt.[50,51]

Procedure for UV-Vis Measurements: Samples were prepared by beginning with a 15 mM solution of **3** under an inert atmosphere. This solution (2-3 mL) was transferred into a gastight cuvette with a septum to allow gas addition. Spectra were collected after the sequential addition of approximately 2 equivalents of O_2 via a gastight syringe until a total of 10 equivalents of O_2 had been added. The solution was purged with N_2 by passing N_2 gas through the solution for 5 minutes, and another spectrum was collected.

Procedure for Cyclic Voltammetry (CV) Measurements: All cyclic voltammetry scans were collected in triplicate at a scan

rate of 50 mV/s and referenced using an Ag/AgCl electrode with a porous Teflon tip stored in a 1M KCl solution. A glassy carbon working electrode with a 3 mm diameter was used and polished with alumina before each scan, and a platinum wire was used as the counter electrode. Sodium phosphate (NaPi) buffer stock solutions were prepared using sodium monobasic phosphate (NaH_2PO_4) and sodium dibasic phosphate (Na_2HPO_4). The pH of each stock solution was adjusted using NaOH or HCl as appropriate and confirmed using a 3-point calibrated Mettler Toledo FiveEasy pH meter. Solutions were deoxygenated as necessary by passing N_2 gas through both stock and experimental solutions before performing each experiment. For all variable pH experiments, a 0.5 mM solution of complex **3** was prepared by dissolving **3** in 0.1 M NaPi buffer at the desired pH. Scans of these solutions were collected under N_2. For the two rinse test experiments, the following procedure was used: first, a scan of deoxygenated 0.1 M NaPi buffer solution at pH 7 was collected under N_2. A separate solution of 0.5 mM complex **3** was prepared using a 0.1M NaPi buffer solution at pH 7, and either a CV or a controlled potential electrolysis scan of this solution at 1.25 V vs. Ag/AgCl was collected under N_2. In both cases, after the experiment the glassy carbon working electrode was rinsed with water but was not polished with alumina before collecting another scan of deoxygenated 0.1 M NaPi buffer solution at pH 7 under N_2. For all poisoning experiments, the following procedure was used: a 2.0 mM stock solution of complex **3** was prepared using 0.1 M NaPi buffer at pH 7. A 2.0 mM stock solution of 2,2'-bipyridine poison was prepared using 0.1 M NaPi buffer at pH 7. These two stock solutions and the 0.1 M NaPi buffer solution were combined in proportions appropriate to obtain 0, 1, 2, or 3 equivalents of the 2,2'-bipyridine poison relative to complex **3**. Scans of the resulting solutions were collected under N_2. For KIE experiments, a stock solution of 0.1 M NaPi buffer was prepared in D_2O at pD 8.5. The pD was measured using a Mettler Toledo FiveEasy pH meter and verified by aligning the $E_{1/2}$ of the Co^{II}/Co^{III} couples in D_2O to those measured in H_2O. A 0.5 mM solution of complex **3** was prepared by dissolving **3** in the D_2O NaPi stock solution. Scans were collected under N_2. The KIE was calculated from $(i_{H2O}/i_{D2O})^2$ since k_{cat} is proportional to i_{cat}^2. For the measurements with variable buffer concentration, a stock solution of pH 8.5 NaPi buffer was prepared at the desired concentration of HPO_4^{2-} (0.095 M, 0.060 M, or 0.030 M) and NaCl was added to maintain an ionic strength of 0.29 M. A 0.5 mM solution of **3** was prepared by dissolving **3** in the appropriate buffer and CV scans were collected in triplicate under N_2.

Procedure for Oxygen Evolution and Controlled Potential Electrolysis Measurements

Dissolved O_2 evolved during controlled-potential electrolyses was quantified using a Unisense Microsensor Monometer equipped with an Ox-500 oxygen probe. A three-point calibration was established with N_2-sparged (0%), air-saturated (20.8% O_2), and O_2-sparged (100%) solutions. The dissolved O_2 concentration in solution at 20°C was determined from a linear interpolation of solubility data reported at 20°C: $[O_2]_{air\text{-}saturated}$ = 0.26 mM and $[O_2]_{oxygen\text{-}saturated}$ =1.25 mM in pH 7 buffer. Controlled-potential electrolyses were conducted in a custom two-compartment H-cell shown in the SI. The first compartment was airtight and contained a 0.25 cm diameter glassy-carbon rod working electrode with ~3 cm in contact with electrolyte solution (~4.9 cm^2 surface area), Ag/AgCl reference electrode (CH-Instruments), a small stir bar, and an Ox-500 oxygen probe (Unisense A/S) with a total volume of 54 mL. The second compartment contained a Pt mesh counter electrode (Alfa Aesar). The two compartments were separated by a Nafion 117 membrane (t = 0.007 in., Sigma-Aldrich). Both compartments were filled with air-saturated 0.1 M NaPi solution. The first compartment was filled specifically such that there was no appreciable headspace. The concentration of dissolved O_2 was monitored for 10 min at open circuit potential (OCP), followed by a controlled potential electrolysis of complex **3**, where the potential was held at 1.25 V vs Ag/AgCl for 10 min passing a total charge of *ca.* 2.5 C. The O_2 produced was calculated by taking the difference between the measured equilibrated O_2 concentration five minutes after the end of the electrolysis and the background O_2 (at OCP). The Faradaic efficiency was calculated by taking the increase of the dissolved O_2 divided by the theoretical value calculated from the total charge passed. Control experiments were carried out using the same procedure (See SI).

Procedure for X-ray Photoelectron Spectrum (XPS) Measurements. XPS spectra were acquired on a Kratos Axis Ultra XPS with a monochromatic Al Kα X-ray source (1486.7 eV) operating at 8 mA and 14 kV. The peak positions of the XPS peaks were referenced against the graphitic/advantageous carbon peak that occurred at 284.8 eV. Any charging effects during data acquisition were compensated using an electron flood gun. Survey scans were collected using a pass energy of 160 and step size of 1 eV (See SI). High-resolution core scans were collected at a pass energy of 20 and step size of 0.1 eV (See SI). For the quantitative determination of that elemental ratios, peaks from high-resolution XPS core scans were fitted to symmetric Voigt line shapes composed of Gaussian (70%) and Lorentzian (30%) functions with a Shirley background using the CasaXPS version 2.3.17 software (Casa Software Ltd). Elemental ratios were calculated by quantifying the total peak area in the N 1s region, the O 1s region, the Co $2p_{3/2}$ peak and associated shake-up peak, the Na 2s region, the P $2p_{3/2}$ peak, and the C 1s region and dividing by their respective relative sensitivity factors (as tabulated for the Kratos Ultra XPS instrument). The ratio of the resulting corrected peak areas is shown in Table S2 with the Co peak area set to 1.

ASSOCIATED CONTENT

Supporting Information

Supplementary figures are given in the supporting information which is available free of charge via the Internet at http://pubs.acs.org.

AUTHOR INFORMATION

Corresponding Author

*E-mail: jsanderson@uchicago.edu

Author Contributions

The manuscript was written through contributions of all authors. All authors have given approval to the final version of the manuscript. ‡These authors contributed equally. † Current Address: National Taiwan University, Department of Chemistry, No. 1 Section 4 Roosevelt Road, Taipei City, Da'an District, TW 10.

Notes

The authors declare no competing financial interests.

ACKNOWLEDGMENT

NDM, AWW, MKG, M-CC, and JSA were funded by the University of Chicago Department of Chemistry and by the National Science Foundation (Grant #CAT-1654144). C-CL, W-JF, and CCLM were funded by the University of Michigan. XPS measurements were conducted at the Michigan Center for Materials Characterization with support from the University of Michigan College of Engineering and the National Science Foundation (Grant #DMR-0420785).

REFERENCES

1. Nocera, D. G. The Artificial Leaf. *Acc. Chem. Res*. **2012**, *45*, 767–776.
2. Concepcion, J.; House, R.; Papanikolas, J.; Meyer, J. Chemical approaches to artificial photosynthesis. *Proc. Natl. Acad. Sci. U. S. A.* **2012**, *109*, 15560-15564.
3. Lewis, N. S. Research opportunities to advance solar energy utilization. *Science*. **2016**, *351,* 1672.
4. Eisenberg, R.; Gray, H. B. Preface to Making Oxygen. *Inorg. Chem.* **2008**, *47*, 1697-1699.
5. McKone, J. R.; Lewis, N. S.; Gray, H. B. Will Solar-Driven Water-Splitting Devices See the Light of Day? *Chem. Mater*. **2014**, *26*, 407-414.
6. Shaffer, D.; Xie, Y.; Concepcion, J. O-O bond formation in ruthenium-catalyzed water oxidation: single-site nucleophilic attack vs. O-O radical coupling. *Chem. Soc. Rev.* **2017**, *46*, 6170-6193.
7. McCrory, C.; Jung, S.; Peters, J.; Jaramillo, T. Benchmarking Heterogeneous Electrocatalysts for the Oxygen Evolution Reaction *J. Am. Chem. Soc.* **2013**, *135*, 16977-16987.
8. McCrory, C.; Jung, S.; Ferrer, I.; Chatman, S.; Peters, J.; Jaramillo, T. Benchmarking hydrogen evolving reaction and oxygen evolving reaction electrocatalysts for solar water splitting devices. *J. Am. Chem. Soc.* **2015**, *137*, 4347-4357.
9. Suen, N.-T.; Hung, S.-F.; Quan, Q.; Zhang, N.; Xu, Y.-J.; Chen, H. M. Electrocatalysts for the oxygen evolution reaction: recent development and future perspectives. *Chem. Soc. Rev.* **2017**, *46*, 337-365.
10. Kanan, M.; Nocera, D. G. In Situ Formation of an Oxygen-Evolving Catalyst in Neutral Water Containing Phosphate and Co^{2+}. *Science*, 2008, **321**, 1072–1076.
11. Pokhrel, R.; Goetz, M. K.; Shaner, S. E.; Wu, X.; Stahl, S. S. The "Best Catalyst" for Water Oxidation Depends on the Oxidation Method Employed: A Case Study of Manganese Oxides. *J. Am. Chem. Soc.* **2015**, *137*, 8384-8387.
12. Han, L.; Dong, S.; Wang, E. Transition-Metal (Co, Ni, and Fe)-Based Electrocatalysts for the Water Oxidation Reaction. *Adv. Mater.* **2016**, *28*, 9266-9291.
13. Hunter, B. M.; Gray, H. B.; Müller, A. M. Earth-Abundant Heterogeneous Water Oxidation Catalysts. *Chem. Rev.* **2016**, *116*, 14120-14136.
14. Montoya, J. H.; Seitz, L. C.; Chakthranont, P.; Vojvodic, A.; Jaramillo, T. F.; Norskov, J. K. Materials for solar fuels and chemicals. *Nat. Mater.* **2016**, *16*, 70-81.
15. Surendranath, Y.; Kanan, M. W.; Nocera, D. G. Mechanistic studies of the oxygen evolution reaction by a cobalt-phosphate catalyst at neutral pH. *J. Am. Chem. Soc.* **2010**, *132*, 16501-16509.
16. Gerken, J. B.; McAlpin, J. G.; Chen, J. Y. C.; Rigsby, M. L.; Casey, W. H.; Britt, R. D.; Stahl, S. S. Electrochemical water oxidation with cobalt-based electrocatalysts from pH 0-14: the thermodynamic basis for catalyst structure, stability, and activity. *J. Am. Chem. Soc.* **2011**, *133*, 14431-14442.
17. Smith, R. D. L.; Prévot, M. S.; Fagan, R. D.; Trudel, S.; Berlinguette, C. P. Water oxidation catalysis: electrocatalytic response to metal stoichiometry in amorphous metal oxide films containing iron, cobalt, and nickel. *J. Am. Chem. Soc.* **2013**, *135*, 11580-11586.
18. Ullman, A. M.; Brodsky, C. N.; Li, N.; Zheng, S.-L.; Nocera, D. G. Probing Edge Site Reactivity of Oxidic Cobalt Water Oxidation Catalysts. *J. Am. Chem. Soc.*, **2016**, *138*, 4229-4236.
19. Goldsmith, Z. K.; Harshan, A. K.; Gerken, J. B.; Voros, M.; Galli, G.; Stahl, S. S.; Hammes-Schiffer, S. Characterization of NiFe oxyhydroxide electrocatalysts by integrated electronic structure calculations and spectroelectrochemistry. *Proc. Natl. Acad. Sci. U. S. A.* **2017**, *114*, 3050-3055.
20. Nguyen, A. I.; Suess, D. L. M.; Darago, L. E.; Oyala, P. H.; Levine, D. S.; Ziegler, M. S.; Britt, R. D.; Tilley, T. D. Manganese-Cobalt Oxido Cubanes Relevant to Manganese-Doped Water Oxidation Catalysts. *J. Am. Chem. Soc.* **2017**, 139, 5579-5587.
21. Swierk, J. R.; Tilley, T. D. Electrocatalytic Water Oxidation by Single Site and Small Nuclearity Clusters of Cobalt. *J. Electrochem. Soc.* **2018**, *165*, H3028-H3033.
22. Concepcion, J. J.; Jurss, J. W.; Brennaman, M. K.; Hoertz, P. G.; Patrocinio, A. O. T.; Iha, N. Y. M.; Templeton, J. L.; Meyer, T. J. Making oxygen with ruthenium complexes. *Acc. Chem. Res.* **2009**, *42*, 1954-1965.
23. Wasylenko, D. J.; Palmer, R. D.; Berlinguette, C. P. Homogeneous water oxidation catalysts containing a single metal site. *Chem. Comm.* **2013**, *49*, 218-227.
24. Kärkäs, M. D.; Verho, O.; Johnston, E. V.; Åkermark, B. Artificial photosynthesis: molecular systems for catalytic water oxidation. *Chem. Rev.* **2014**, *114*, 11863-12001.
25. Blakemore, J. D.; Crabtree, R. H.; Brudvig, G. W. Molecular catalysts for water oxidation. *Chem. Rev.* **2015**, *115*, 12974-13005.
26. Walden, A. G.; Miller, A. J. M. Rapid water oxidation electrocatalysis by a ruthenium complex of the tripodal ligand tris(2-pyridyl)phosphine oxide. *Chem. Sci.* **2015**, *6*, 2405-2410
27. Meyer, T. J.; Sheridan, M. V.; Sherman, B. D. Mechanisms of molecular water oxidation in solution and on oxide surfaces. *Chem. Soc. Rev.* **2017**, *46*, 6148-6169.
28. Liao, R.-Z.; Siegbahn, P. E. M. Quantum Chemical Modeling of Homogeneous Water Oxidation Catalysis. *ChemSusChem*. **2017**, *10*, 4236-4263.
29. Limburg, J.; Vrettos, J. S.; Chen, H.; de Paula, J. C.; Crabtree, R. H.; Brudvig, G. W. Characterization of the O_2-evolving Reaction Catalyzed by $[(terpy)(H_2O)Mn^{III}(O)_2Mn^{IV}(OH_2)(terpy)]$ $(NO_3)_3$. *J. Am. Chem. Soc.* **2001**, *123*, 423-430.
30. Ellis, W. C.; McDaniel, N. D.; Bernhard, S.; Collins, T. J. Fast Water Oxidation Using Iron. *J. Am. Chem. Soc.* **2010**, *132*, 10990-10991.
31. Barnett, S.; Goldberg, K.; Mayer, J. A soluble copper-bipyridine water-oxidation electrocatalyst. *Nat. Chem.* **2012**, *4*, 498–502.
32. Singh, A.; Spiccia, L. Water oxidation catalysts based on abundant 1st row transition metals. *Coord. Chem. Rev.* **2013**, *257*, 2607-2622.
33. Zhang, T.; Wang, C.; Liu, S.; Wang, J.-L.; Lin, W. A Biomimetic Copper Water Oxidation Catalyst with Low Overpotential. *J. Am. Chem. Soc.* **2014**, *136*, 273-281.
34. Lee, W.-T.; Muñoz, S. B.; Dickie, D. A.; Smith, J. M. Ligand Modification Transforms a Catalase Mimic into a Water Oxidation Catalyst. *Angew. Chem. Int. Ed.* **2014**, *53*, 9856-9859.
35. Dogutan, D.; McGuire, R.; Nocera, D. G. Electrocatalytic Water Oxidation by Cobalt(III) Hangman β-Octafluoro Corroles. *J. Am. Chem. Soc.* **2011**, *133*, 9178–9180.
36. Lv, H. J.; Geletii, Y. V.; Zhao, C. C.; Vickers, J. W.; Zhu, G. B.; Luo, Z.; Song, J.; Lian, T. Q.; Musaev, D. G.; Hill, C. L. Polyoxometalate water oxidation catalysts and the production of green fuel. *Chem. Soc. Rev.* **2012**, *41*, 7572-7589.
37. Rigsby, M.; Mandal, S.; Nam, W.; Spencer, L.; Llobet, A.; Stahl, S. S. Cobalt analogs of Ru-based water oxidation catalysts: Overcoming thermodynamic instability and kinetic lability to achieve electrocatalytic O_2 evolution. *Chem. Sci.* **2012**, *3*, 3058.
38. Wang, D.; Groves, J. Efficient water oxidation catalyzed by homogeneous cationic cobalt porphyrins with critical roles for the buffer base. *Proc. Natl. Acad. Sci. U. S. A.* **2013**, *110*, 15579–15584.
39. Pizzolato, E.; Natali, M.; Posocco, B.; Lopez, A. M.; Bazzan, I.; Di Valentin, M.; Galloni, P.; Conte, V.; Bonchio, M.; Scandola, F.; Sartorel, A. Light driven water oxidation by a single site cobalt salophen catalyst. *Chem. Commun.* **2013**, *49*, 9941-9943.
40. Fu, S.; Liu, Y.; Ding, Y.; Du, X.; Song, F.; Xiang, R.; Ma, B. A mononuclear cobalt complex with an organic ligand acting as a precatlyst for efficient visible light-driven water oxidation. *Chem. Commun.* **2014**, *50*, 2167-2169.
41. Kotyk, J.; Hanna, C.; Combs, R.; Ziller, J.; Yang, J. Intramolecular hydrogen-bonding in a cobalt aqua complex and electrochemical water oxidation activity. *Chem. Sci.* **2018**, *9*, 2750-2755.
42. Jonas, R.; Stack, T. C-H Bond Activation by a Ferric Methoxide Complex: A Model for the Rate-Determining Step in the Mechanism of Lipoxygenase. *J. Am. Chem. Soc.* **1997**, *119*, 8566–8567.
43. de Vries, M.; La Crois, R.; Roelfes, G.; Kooijman, H.; Spek, A.; Hage, R.; Feringa, B. A novel pentadentate ligand 2,6-bis[methoxybis(2-pyridyl)methyl]pyridine L for mononuclear iron(II) and manganese(II) compounds. *Chem. Commun.* **1997**, *16*, 1549–1550.
44. Wasylenko, D.; Ganesamoorthy, C.; Borau-Garcia, J.; Berlinguette, C. Electrochemical evidence for catalytic water oxidation mediated by a high-valent cobalt complex. *Chem. Comm.* **2011**, *47*, 4249-4251.

45. Sun, Y.; Bigi, J.; Piro, N.; Tang, M.-L.; Long, J. R.; Chang, C. J. Molecular Cobalt Pentapyridine Catalysts for Generating Hydrogen from Water. *J. Am. Chem. Soc.* **2011**, *133*, 9212-9215.
46. Wasylenko, D.; Palmer, R.; Schott, E.; Berlinguette, C. Interrogation of electrocatlytic water oxidation mediated by a cobalt complex. *Chem. Comm*. **2012**, *48*, 2107.
47. Crandell, D. W.; Ghoush, S.; Berlinguette, C. P.; Baik, M.-H. How a [Co(IV) a bond and a half O](2+) fragment oxidizes water: involvement of a biradicaloid [Co(II)-(·O·)](2+) species in forming the O-O bond. *ChemSusChem*. **2015**, *8*, 844-852.
48. Siewert, I.; Gałęzowska, J. Cobalt Catalyst with a Proton-Responsive Ligand for Water Oxidation. *Chem. Eur. J*. **2015**, *21*, 2780–2784.
49. Wilken, M.; Würtele, L.; Kügler, M.; Chrobak, F.; Siewert, I. Thermochemistry of a Cobalt Complex with Ionisable Pyrazole Protons. *Eur. J. Inorg. Chem.* **2018**, *20-21*, 2339-2344.
50. Takano, S.; Yano, Y.; Tagaki, W. Synthesis of Some New Ligands Containing Imidazoles and Reversible Oxygenation of the Cobalt(II) Complexes. *Chem. Lett.* **1981**, *8*, 1177–1180.
51. S. Tamagaki, S.; Y. Kanamaru, Y.; M. Ueno, M.; W. Tagaki, W. Physical and Chemical Properties of Mononuclear Cobalt Dioxygen Complexes with Tetraimidazolyl-Substituted Pyridine Chelates. *Bull. Chem. Soc. Jpn.*, 1991, **64**, 165–174.
52. Ullman, A. M.; Liu, Y.; Huynh, M.; Bediako, D. K.; Wang, H.; Anderson, B. L.; Powers, D. C.; Breen, J. J.; Abruña, H. D.; Nocera, D. G. Water Oxidation catalysis by Co(II) impurities in $Co(III)_4O_4$ cubanes. *J. Am. Chem. Soc.* **2014**, *136*, 17681-17688.
53. Stracke, J. J.; Finke, R. G. Distinguishing Homogeneous Water Oxidation Catalysis when Beginning with Polyoxometalates. *ACS Catal.* **2014**, *4*, 909-933.
54. Kaeffer, N.; Morozan, A.; Fize, J.; Martinez, E.; Guetaz, L.; Artero, V. The Dark Side of Molecular Catalysis: Diimine-Dioxime Cobalt Complexes Are Not the Actual Hydrogen Evolution Electrocatalyst in Acidic Aqueous Solutions. *ACS Catal*. **2016**, *6*, 3727-3737.
55. Wang, J.-W.; Sahoo, P.; Lu, T.-B. Reinvestigation of Water Oxidation Catalyzed by a Dinuclear Cobalt Polypyridine Complex: Identification of CoO_x as a Real Heterogeneous Catalyst. *ACS. Catal*. **2016**, *6*, 5062-5068.
56. Sconyers, D. J.; Blakemore, J. D. Distinguishing between homogeneous and heterogeneous hydrogen-evolution catalysis with molecular cobalt complexes. *Chem. Comm.* **2017**, *53*, 7286-7289.
57. Coggins, M. K.; Zhang, M.-T.; Chen, Z.; Song, N.; Meyer, T. J. Single-Site Copper(II) Water Oxidation Electrocatalysis: Rate Enhancements with HPO_4^{2-} as a Proton Acceptor at pH 8. *Angew. Chem., Int. Ed.* **2014**, *53*, 12226-12230.
58. Li, X.; Zhan, C.; Wang, Y.; Yao, J. Pyridine-imide oligomers. *Chem. Comm.* **2008**, *21*, 2444-2448.
59. Angelici, R. J. Ed. *Dodecacarbonyltriosmium*; Inorganic Syntheses: John Wiley & Sons, Inc., Hoboken, NJ, USA, 1990.

A previously reported cobalt complex featuring a tetraimidazolyl-substituted pyridine chelate is an active water oxidation electrocatalyst with moderate overpotential at pH 7. Cyclic voltammetry measurements confirm that the imidazolyl donors result in a more electron-rich Co center when compared with previous pyridine-based systems. The primary changes in electrocatalytic behavior of the present case are enhanced activity at lower pH and a marked dependence of catalytic activity on pH.

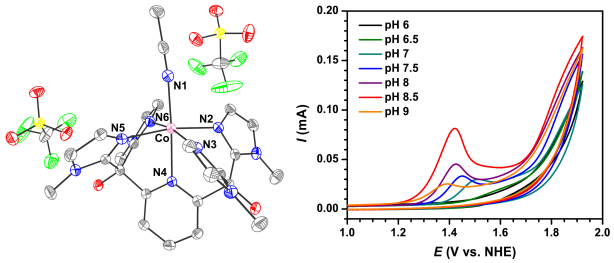

Rate Determining PCET in Water Oxidation Electrocatalysis
